SDC-91-00051

SDC
SOLENOIDAL DETECTOR NOTES

b-Jet Tagging Using Electrons at SDC

A. B. Wicklund

14 AUGUST 1991

SDC-91-00051
ANL-HEP-TR-91-70

b-Jet Tagging Using Electrons at SDC*

A. B. Wicklund
14 August 1991

This note examines b-jet tagging at SDC, using semileptonic $b \rightarrow e\upsilon X$ electron decays. The main application for this tagging capability would be in the study of Top decays. Thus, we consider Top decays in a "reasonable" mass range (e.g. $110 < Mtop < 170$). For completeness, we also consider inclusive QCD production of b-quarks. We are mainly interested in the effects of hadron calorimeter segmentation on the electron efficiency, assuming that similar algorithms are used for electron ID at SDC as at CDF. We review the following topics:

1) Kinematics of Top decay;

2) Kinematics of semileptonic b-decay;

3) Effects of Had/EM cuts on electron ID, as a function of b-decay kinematics and calorimeter segmentation;

4) Overall efficiency for b-tagging from Top decay and inclusive b-production.

We consider only the barrel region in our simulation, e.g. $\eta < 1.4$.

1) Top Kinematics

The Pt spectrum for b-jets in $Top \rightarrow b + W$ is much harder than the corresponding spectrum for QCD production of $\bar{b}b$. Figure (1) shows the Pt spectrum for Mtop = 140 (histograms). The mean Pt is around 50 GeV/c, corresponding to the jacobean peak in $Top \rightarrow b + W$. We have used lowest order Papageno to derive Fig. (1), but we expect that NLO corrections will not affect the spectral shape much. To a good approximation, the spectrum scales as the center-of-mass momentum in $Top \rightarrow b + W$. Figure (1) shows the Pt (b) spectrum for Mtop = 110 (a) and Mtop = 170 (b) (points with error bars); here we have scaled up the Pt (b) values in each case by the ratio of CM momentum, i.e.

$$Pt\,(b)\ plotted = Pt\,(b)\,(Mtop) \times Q(140)/Q(Mt)$$

This scaling behavior is convenient in describing the ***SHAPE*** of the Pt (b) spectrum; of course the Top cross section falls with Mtop, but that is irrelevant for our analysis.

Figure (2) compares rates for inclusive direct b-quark production and Top decay to b-quark, as a function of Pt (b). The rates are based on the Nason et al. predictions (courtesy of R. Meng), integrated over $\eta < 1.5$ (b quark only). Also shown in Fig. (2) is the typical expected efficiency for electron ID, based on a simple cut on Had/Em (longitudinal shower development) and a requirement that the decay electron have Pt > 7 GeV/c (see below). This efficiency is fairly flat in Pt, and applies equally to both sources of b-quarks. Overall, the direct b-production rates exceed those from 140 GeV Top by 2-3 orders of magnitude, in the absence of any additional cuts (e.g. presence of $W \rightarrow e\ \nu$) used to flag Top decays.

2) b-Quark Decay Kinematics

Given the Pt(b) spectrum, we can predict the lepton spectrum by convoluting the $b \rightarrow B$ fragmentation distribution (using Petersen fragmentation with $\langle z \rangle = 0.83$, consistent with PEP/PETRA/LEP data), and the $B \rightarrow e^{\pm}$ spectrum using CLEO data. Experimentally, we are mainly interested in the $b \rightarrow$ electron kinematical efficiency, for a fixed threshold cut on the electron Pt. Figure (3) shows the integral probability (in parts per mil) for detecting the electron as a function of Pt (b); the curves are for Pt (electron) thresholds between 2 and 20 GeV/c, in steps of 2 GeV/c. For example, a 50 GeV b-quark would have 90% efficiency for an electron cut at 2 GeV/c, and 10% for an electron cut at 20 GeV/c. At CDF, with a 12 GeV/c electron threshold, the QCD production of b quarks gives an average Pt (b) = 33 GeV. The b-quarks at SDC, from decay of a 140 GeV Top, peak at around 50 GeV/c, so that an electron threshold of 12 GeV/c would be fairly reasonable.

The kinematical efficiency curves in Fig. (3) scale approximately in the variable Pt (e)/Pt (b), where Pt (e) is the electron threshold. Figure (4) shows the same integral curves, for 2 GeV/c threshold (points), and for 8-20 GeV/c thresholds (solid curves). The 8-20 GeV/c curves have been scaled down by using

$$\text{Pt (plotted)} = \text{Pt (b)} \ \ \text{X} \ \ 2\ (\text{GeV/c})/P_t\ (\text{electron}),$$

i.e. so as to correspond to the 2 GeV/c threshold. The higher Pt electron cutoffs all fall on the same curve; the 2 GeV/c points differ slightly from this curve due to threshold effects involving finite b-quark mass.

Thus, for any top mass, it is straightforward to compute the probability for tagging the top using $b \rightarrow$ electron, with the electron above a fixed Pt cutoff. The scaling behaviour in the top decay spectrum and in the b-quark fragmentation makes this quite simple; it is just a matter of convoluting the b-quark spectrum from the Top decay with the probability of finding an electron above a Pt cutoff.

3) Detection Efficiency: Ideal Calorimeter

In CDF, b-tagging with electrons makes use of Had/Em cuts (at the trigger level) and cuts on lateral shower development at shower max., using the CDF strip chambers. The shower max. detector gives shower shape, track position matching, and pulse height over a relatively small part of the EM calorimeter (the electron shower profile is effectively contained in ± 6 cm at 6 X0); in addition, the CDF algorithms are constructed so as to search, in effect, for additional EM shower energy away from the "electron", in order to remove hadron photon "overlap" events. Empirically, the shower max response is very similar for electrons and early showering hadrons, and it is the ***SHAPE*** of the Had/Em distribution that allows a statistical separation of electron signal from fake hadron background; the electron signal peaks at Had/Em = 0, while the background, depending on shower max. cuts, tends to be flat in Had/Em. The usefulness of Had/Em as a discriminator is limited by the calorimeter granularity and the hadron shower size, and by the hadronic energy leakage from other particles in the b-jet. For discussion purposes, we will assume that cuts are made on Had/Em, using a well-defined fiducial volume for electron ID.

The b-tagging efficiency then depends on two functions:

a) The probability that a b-quark will give a electron above the electron Pt cut, and

b) The probability, averaged over electrons above the electron Pt cut, that the electron will pass a Had/Em cut. The latter depends strongly on the b-jet momentum, which determines both the amount of accompanying hadronic energy and the transverse distribution of that energy in the calorimeter.

To compute the detection efficiency of SDC, we start with a barrel segmentation of:

a) $d(z) = 12$ cm, or $d(\eta) \sim 0.05$,

b) $d(\phi) = 360$ deg/128 cells, or $d(\phi) \sim 0.05$

We reference the cell size to the calorimeter face at P = 210 cm, and assume a magnetic field of 2T with 1.8M effective radius. We then consider the distribution of hadronic energy in a 6×6 cell array, where the electron candidate is in one of the central cells, e.g. (3,3), (3,4), (4,3), or (4,4) in an obvious matrix notation (the 6×6 array is labelled by a matrix (j,k), j = 1,6, k = 1,6). Finally, we consider three algorithms that could be implemented in the trigger or offline:

a) "3×3", using the electron cell and its nearest neighbors.

b) "4 × 4", using 4 × 4 cells in η-ϕ, depending on the location of the electron coil.

c) "6 × 6", using all 6 × 6 cells.

Figure (5) illustrates these configurations. Note that algorithms (b) and (c) could use a 0.1 × 0.1 segmentation of the hadron calorimeter, while (a) requires 0.05 × 0.05 everywhere.

Figure (6) shows the hadronic Pt flow around the electron, as a function of the separation in $R = d(\eta)^2 + d(\phi)^2$, for inclusive b-quarks (e.g. QCD production) produced above 20, 50, and 80 GeV/c Pt thresholds. The integral of each plot gives the average total hadronic energy flow per event. The electron Pt cutoff is chosen to be 12 GeV/c. The collimation of the momentum flow increases with Pt (b), and there is substantial energy flow near the electron (e.g. $R < 0.2$). If we simply register all of the hadronic particle energy in the hadron calorimeter (e.g. Had = Pt, EM = 0), and disregard lateral shower development, we can compute the electron tagging efficiency as a function of Pt (b), for the 3 × 3, 4 × 4, and 6 × 6 algorithms, as shown in Fig. (7). Here we again require Pt (electron) > 12 GeV/c, and we make a requirement (based on CDF) that

Had/EM < 0.04 (Had/EM cut for electron-pion separation.)

The smooth curves in Fig. (7) are polynomial interpolations of the Monte Carlo, used in subsequent efficiency calculations.

We can convolute the Had/Em efficiency with the probability that the electron pass the Pt > 12 GeV/c cut, to obtain the efficiency for Top tagging shown in Fig. (8). In Fig. (8), the curve labelled "all" gives the efficiency if only Pt (e ±) > 12 GeV/c is required; the other curves show the effect of the Had/Em cuts for each algorithm. As a function of the Top mass, the efficiency for the 12 GeV/c electron cut increases with mass (e.g., with Pt (b)), while the efficiency for the Had/EM cuts decreases with mass (again, with increasing Pt (b)).

4) Detection Efficiency: Including Shower Simulation

The hadronic energy deposition is modified by two effects, as compared with the ideal calorimeter simulation described above:

1) Typically (in CDF or SDC), around half of the observed energy is not deposited in the Hadron calorimeter, but rather in the EM, and

2) The hadron showers spread laterally.

We have used single charged particle tracks in CDF to parametrize these effects for b-physics analysis. Figure (9) shows the effective hadron shower size in CDF, defined by

$$dE/dZ = \exp(-Z/\lambda)$$

as a function of charged track momentum and as a function of observed EM/Etot fraction. Hadrons that fake electrons have Em/Etot ~ 1.0, and as might be expected these have broader than average shower spread (15 cm in Fig. (8a)). The shower size refers to a ***PROJECTED*** view in the calorimeter. Mathematically, the radial profile of the shower is given by

$$dE/dR = R \exp(-R/b),$$

where

$$b \approx \lambda \times 3/4$$

This is an approximation of the relevant integrals, which should suffice for the present study. The parameter "λ" can be directly measured in the data, and the corresponding R-dependence can then be used in simulation. To extrapolate from CDF to SDC calorimeters, we scale the showers according to effective absorption length (hadrons) or Moliere radius (electrons), and obtain:

EM shower (SDC) = 0.82 EM shower CDF (Moliere radius),

HAD shower (SDC) = 0.87 HAD shower CDF (absorption length).

We scale the CDF shower profiles by these values, and assume approximate compensation in SDC (e.g. E/p = 1 for hadrons, to be compared with E/p = 0.8 in CDF), to arrive at a simulation of lateral and longitudinal shower development in SDC. This simulation then incorporates the two principal effects noted above (Had/P < 1.0, and lateral spreading).

From Fig. (9), the typical projected HAD shower size in SDC is 8.7 cm* (= 0.87 × 10 cm), so it is clear that a single .05 × .05 cell does not contain a hadronic shower. In the CDF detector, we concatenate three cells ($\eta - \phi = 0.1 \times 0.25$ each) to

---

* Note that the actual "HAD" lateral profile is a strong function of the EM fraction. To compare with other direct measurements of the lateral profile, such as for the ZEUS calorimeter (Nucl Instrum. and Meth. A292, 259 (1990)), one should use the b parameter with EM fraction equal to 0 in Fig. 9. Scaling according to absorption lengths, this b parameter (5 cm in Fig. 9) would be 3.6 cm in the ZEUS setup, to be compared with their testbeam results that give a double exponential profile with $b_1 = 2.0$ cm, $b_2 = 11$ cm, with each contribution having equal integrated rates. The observed HAD profiles, according to Fig. 8, will in general be much broader than this due to the nonzero EM fraction.

form a 0.3×0.35 cell for electron ID and for definition of Had/EM. This larger cell is roughly the size of the ENTIRE 6×6 array that we have considered for SDC. Figure (10) shows 50 GeV pion and electron distributions for Had/EM. The histogram shows the full 3-cell definition, and the points show the corresponding result for a single (0.1×0.25) cell. The testbeam particles are aimed at tower centers, not face-averaged as in the actual experiment. The pion rejection, for any cut on Had/EM consistent with good electron efficiency (e.g. Had/EM < 0.04), is only half as good with the single cell definition. Note that the single cell definition $(.1 \times .25)$ is roughly comparable with the 3×3 algorithm in SDC $(.15 \times .15)$. These are inclusive distributions, and further application of shower max. cuts reduces the pion rates by a factor of three. Depending on shower max. cuts, the final pion rejection is around 30 - 60% worse with the 1-tower as compared with the 3-tower definition.

Simulated Had/EM distributions for SDC $b \rightarrow e + X$ events are shown in Figs. (11, 12, and 13) for QCD b-jets with Pt > 20, 50, and 80 respectively. In each case, the lower subplots (a), (b) are for $b \rightarrow$ electron, so that the hadronic energy deposition is supplied by hadrons in the b-jet. For the top subplots (c), and (d), we have turned the electron into a hadron, allowing it to shower as if it were a pion. By construction, the Had/Em plots for "pions" (fake electrons") are roughly flat. The peak at Had/EM = 0 for real electrons is superposed on a flattish background from hadronic leakage. As expected the electron peak is progressively lost as we increase Pt (b) and increase the cell algorithm from 4×4 to 6×6.

Figures (14) and (15) show the efficiency of the different cell algorithms, for Had/Em < .04 electron cut, versus Pt (b); we have used 7 and 12 GeV electron thresholds for Figs. (14) and (15) respectively. The solid curves are polynomial fits to the efficiencies with no hadron shower simulation (e.g. Fig. (7)). We see that the shower spreading significantly reduces the efficiency for the small cell algorithms (3×3 and 4×4), but has little effect on the 6×6 algorithm; this efficiency reduction is worse at high Pt, where the b-jet has more hadronic energy near the electron.

The dependence of the Had/EM cut efficiency on the electron Pt cut is rather slight. Figure (16) compares the 7 and 12 GeV thresholds for each algorithm. The 7 GeV efficiencies are slightly lower, presumably because there is relatively more hadronic energy, for fixed Pt (b), with the lower electron threshold. Note that the cut on "Had/EM" is defined in all plots as Had/Pt (e), and ignores additional EM energy from the particles accompanying the electron. This allows for sensible comparison of simulated and nonsimulated showers, and is a perfectly reasonable but not unique definition for electron ID. Figure (17) compares the unsimulated and simulated efficiencies for the 12 GeV/c electron cut. The results are smoothed versions of Fig. (14).

The efficiency versus Top mass is shown in Figs. (18) and (19), for the 7 and 12 GeV electron thresholds, with hadron shower simulation for the Had/Em < .04

cut. These figures may be compared with the unsimulated result in Fig. (8). Qualitatively, the main features are as expected:

1) The b-tagging efficiency is significantly higher with the lower (7 GeV) threshold, due to the kinematic efficiency for $b \rightarrow e\,X$.

2) The Had/Em cuts have roughly the same effect for 7 and 12 GeV.

3) The overall efficiencies vary slowly with Mtop, because the kinematic efficiency due to the electron cut increases with Mtop, while the Had/EM cut efficiency decreases.

4) Full hadron simulations gives lower overall efficiency than would be the case for "ideal" calorimeter response ("HAD" = P, no lateral spreading).

5) The efficiency falls smoothly as the algorithm cell size is increased.

5) Conclusions

With realistic hadron slower spreading, the b-jet tagging efficiency is around 20% lower with the "4 × 4" as compared with the "3 × 3" algorithm, and hadron segmentation of .1 × .1 (adequate for "4 × 4" algorithm) is a reasonable match to the expected hadron slower size.

---

* Work supported by the U.S. Department of Energy, Division of High Energy Physics, Contract W-31-109-ENG-38.

FIGURE CAPTIONS

1) Pt spectrum for b-quarks in Top decay for (a) Mt = 110, and (b) Mt = 170. The histograms are for Mt = 140, and the Mt = 110, 170 points are scaled according to the cm momentum in Top decay, to allow comparison with Mt = 140.

2) Cross sections in $\eta < 1.5$ region for inclusive b-quark production (top curve) and Top decay (bottom curve), where the b-quark is required to yield a Pt > 7 GeV/c electron. Also, shown is the average efficiency for identifying the b-quark, including calorimeter Had/EM requirements and kinematical probability for getting 7 GeV electron.

3) Probability in parts per 1000 for getting an electron above indicated threshold (in 2 GeV steps), as a function of b-quark momentum.

4) Same as (3) but with b-quark momentum scaled by electron momentum as explained in text; points are 2 GeV electron efficiency, curves are for 8-20 GeV electrons with scaling.

5) Illustration of cell algorithms used to define Had/Em, for 3×3, 6×6, and 4×4 definitions (1, 2, 3 respectively).

6) Total hadronic Pt flow per event as function of distance R from electron (Pt > 12) in b-quark decay.

7) Efficiencies for Had/Em < .04 cut, as a function of Pt (b-quark), with Pt > 12 required for electron, for the 3×3, 4×4, and 6×6 algorithms. No shower simulation is done (we assume HAD = Pt summed over hadrons). The smooth curves are polynomial fits.

8) Efficiency as function of Mtop with Pt > 12 required for electron; the lower curves include the efficiency of the Had/Em cut with no shower simulation.

9) Shower size parameter versus EM fraction (a) and versus Pt for charged tracks in CDF data.

10) Observed rate for Had/Em distributions for 50 GeV pions (a) and electrons (b) in CDF testbeam. Points are for a η-ϕ = $.1 \times .25$ cell, and histograms for $.3 \times .25$ cell.

11) Simulated Had/Pt distributions for electrons in b-jets (a,b), for Pt (b) > 20, for 4 × 4 and 6 × 6 algorithms; (c,d), same for pions, where we have simply turned the electron in a b-jet into a hadron for display purposes.

12) Same as (11) for Pt (b) > 50.

13) Same as (11) for Pt (b) > 80; Note that the electron "signal" defined by Had/Pt < .04, is reduced in (a) and (b) due to hadron leakage, and also receives more apparent "background", as compared with Figs. (11) and (12).

14) Same as Fig. (7), but for Pt > 7 cut on electron, and hadron shower simulation included. The curves are just the fits shown in Fig. (7) for the case of no shower spreading.

15) Same as (14) for Pt > 12 GeV/c electron cut.

16) Comparison of Had/Pt efficiency as a function of Pt (b) for 7 and 12 GeV/c electron cuts.

17) Comparison of Had/Pt efficiency versus Pt (b) for full shower simulation (solid) and "perfect" calorimeter response (dashed), both for 12 GeV/c electron threshold.

18) Efficiency versus Mtop with full Had/Pt simulation, for 7 GeV electron cut; curves are as in Fig. (8).

19) Same as (18), for 12 GeV/c electron cut.

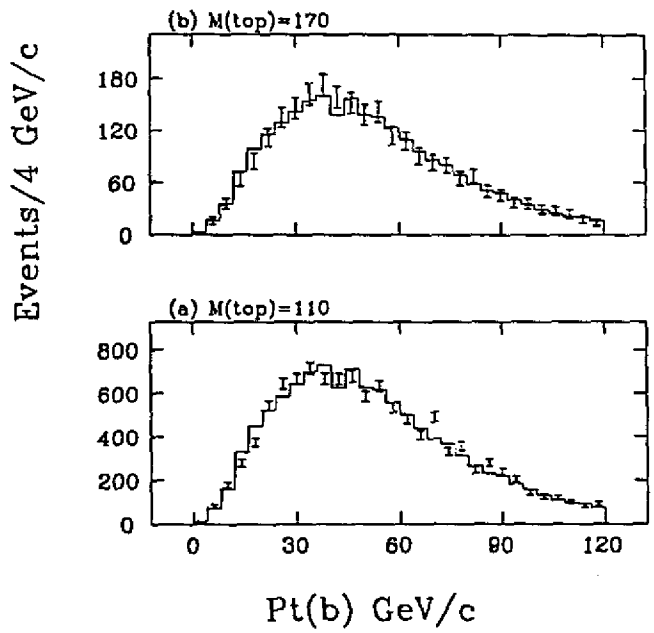

Figure 1

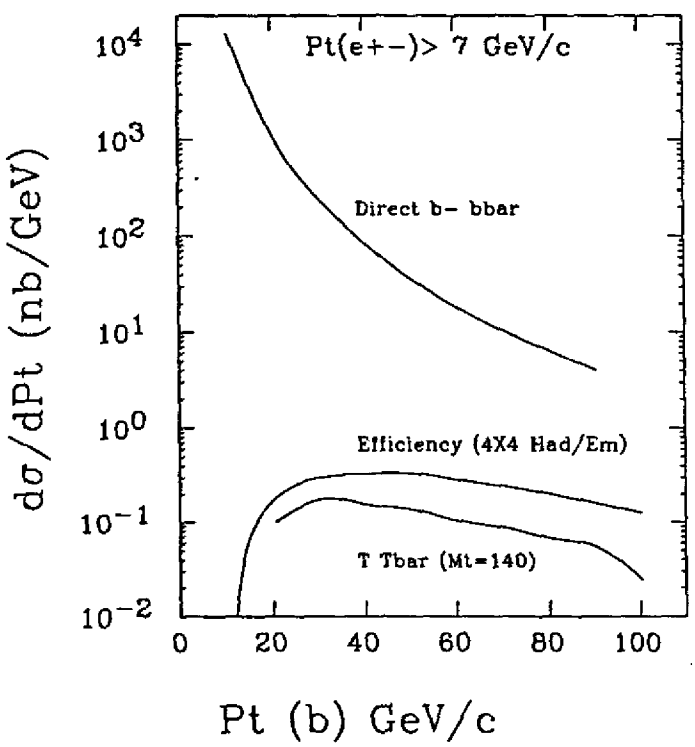

Figure 2

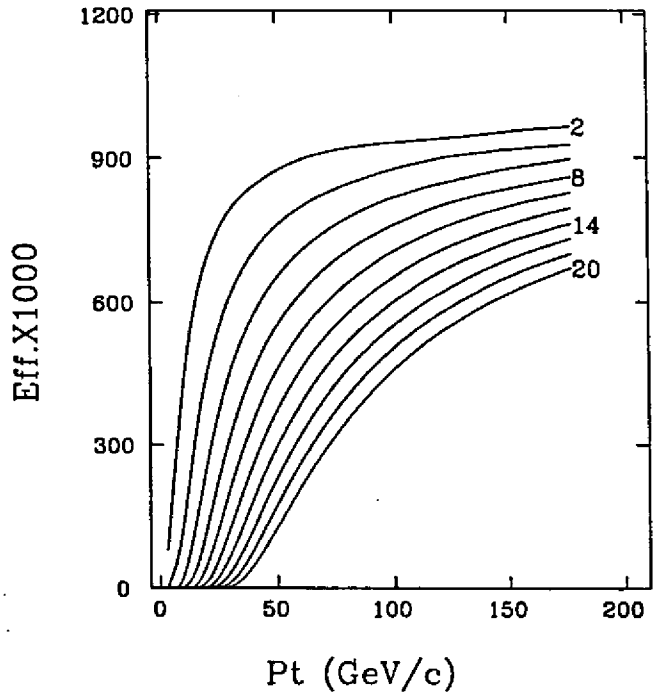

Figure 3

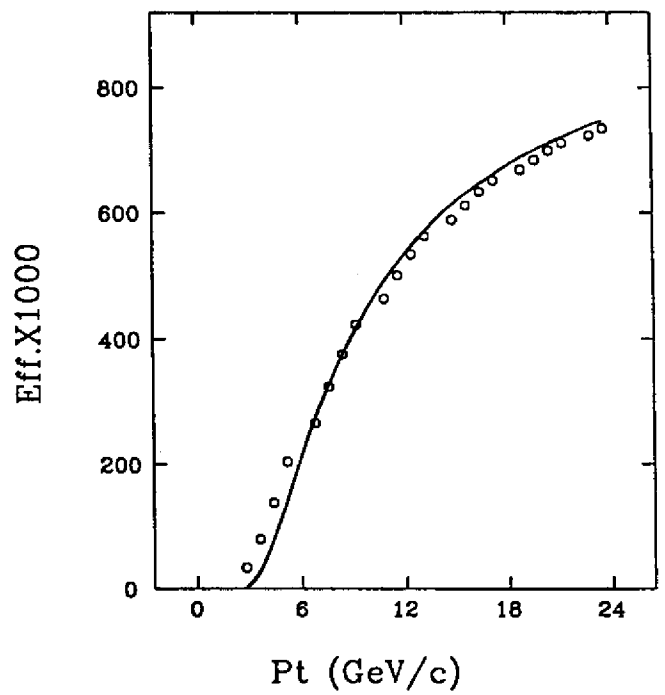

Figure 4

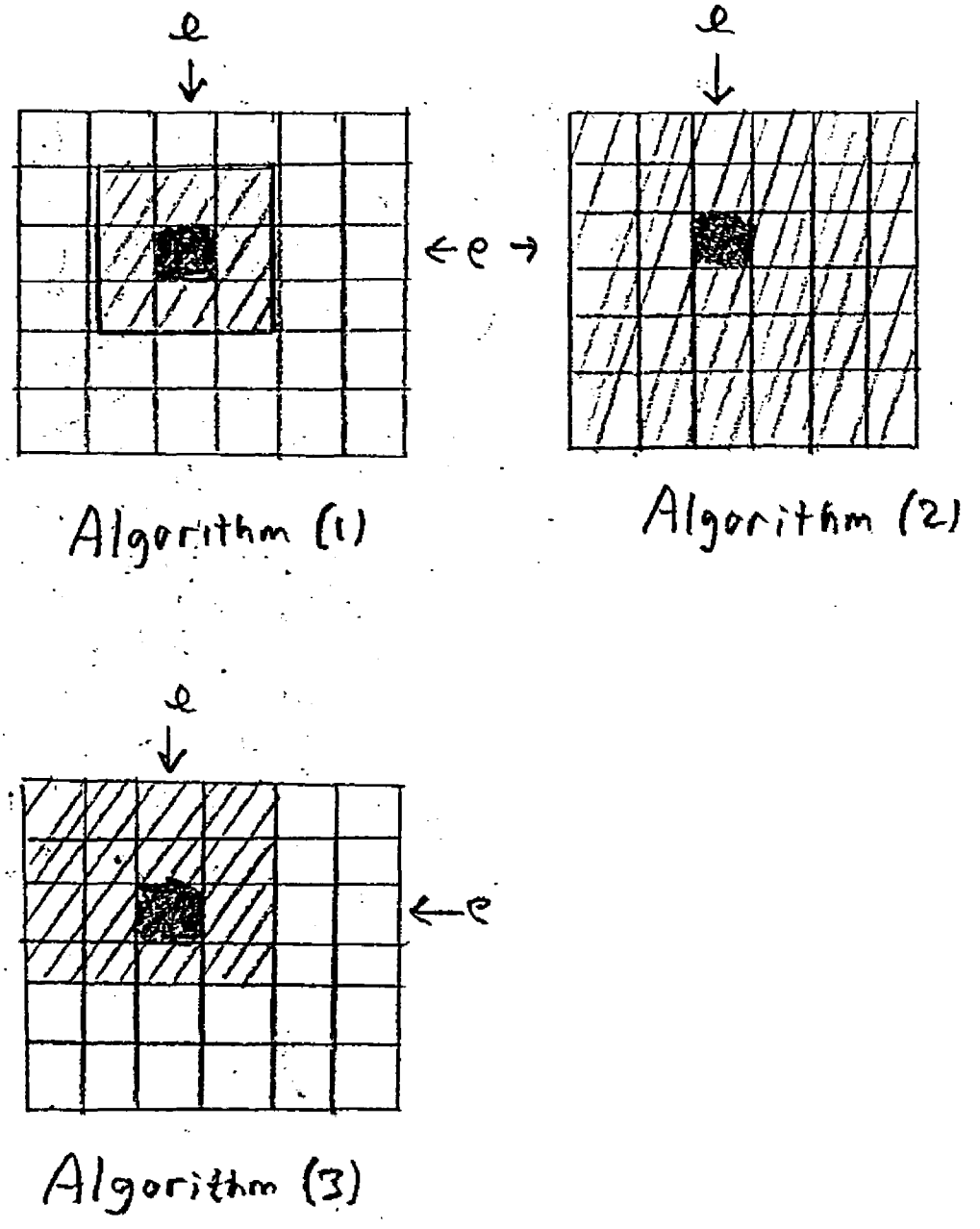

Figure 5

Solid Square = Electron Cell (.05 × .05)
Shaded Region = Definition of Hadron Energy

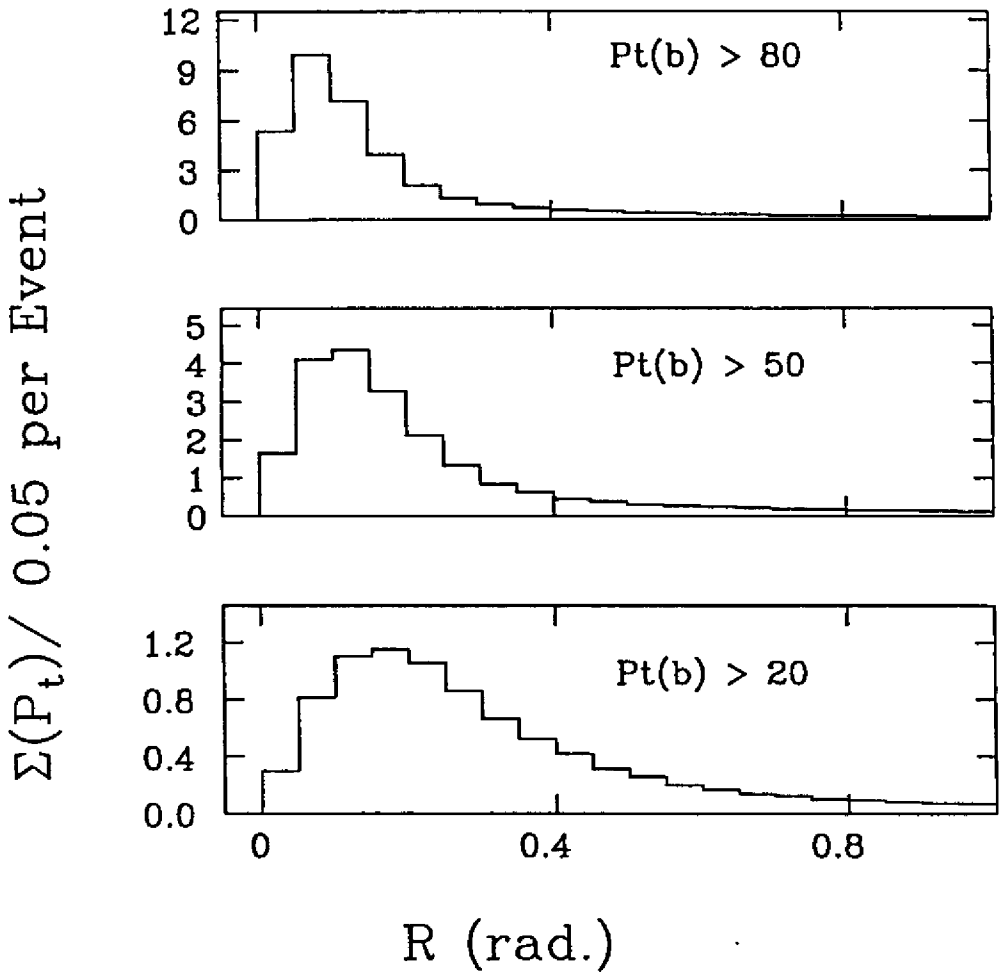
12
9
6
3
0
Pt(b) > 80
5
4
3
2
1
0
Pt(b) > 50
1.2
0.8
0.4
0.0
Pt(b) > 20
0
0.4
0.8
Σ(P_t)/ 0.05 per Event
R (rad.)

Figure 6

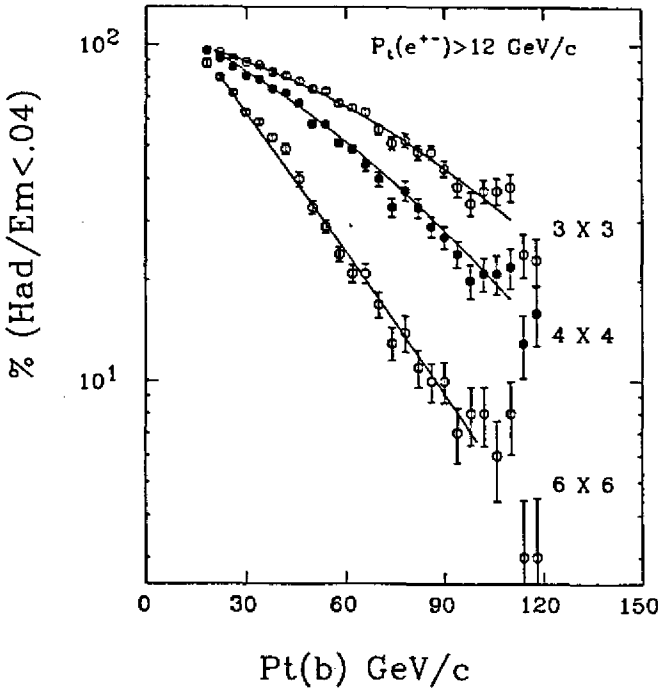

Figure 7

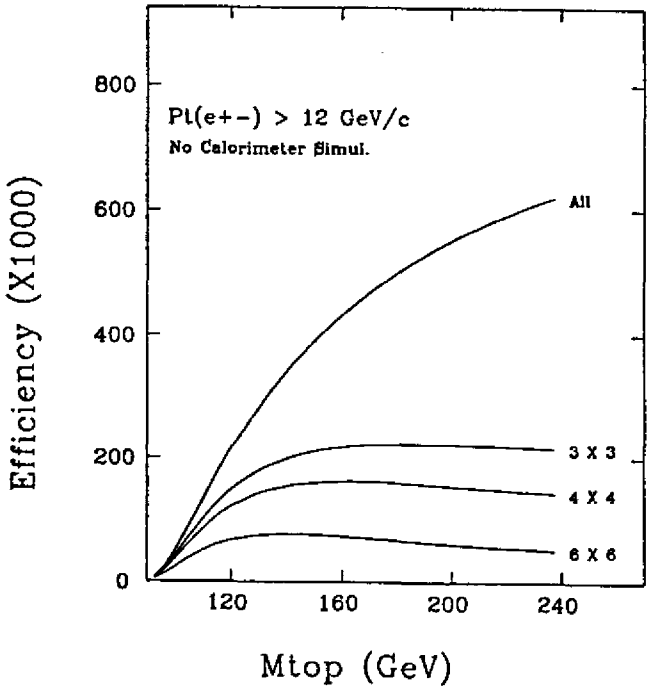

Figure 8

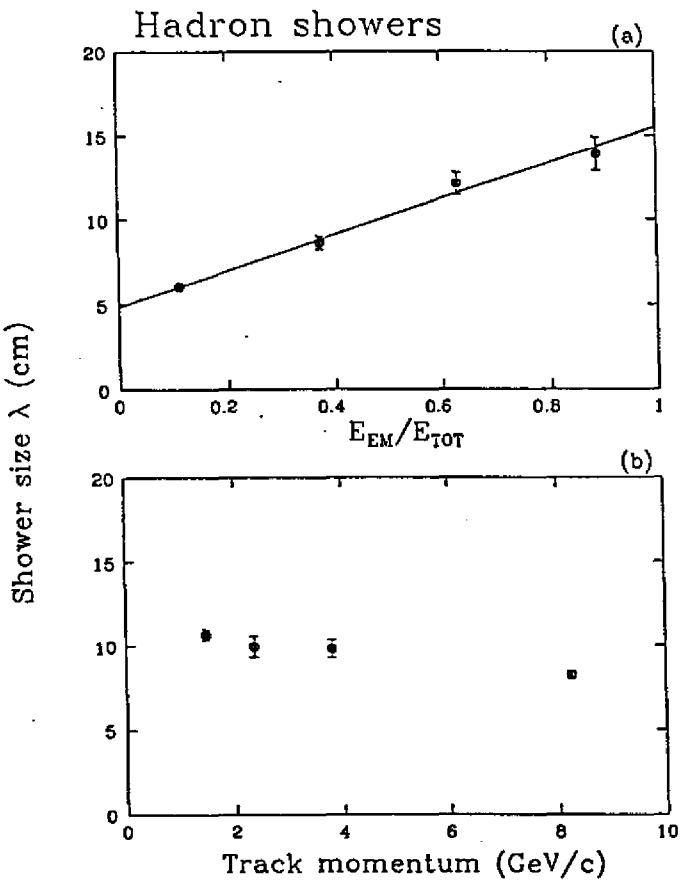

Figure 9

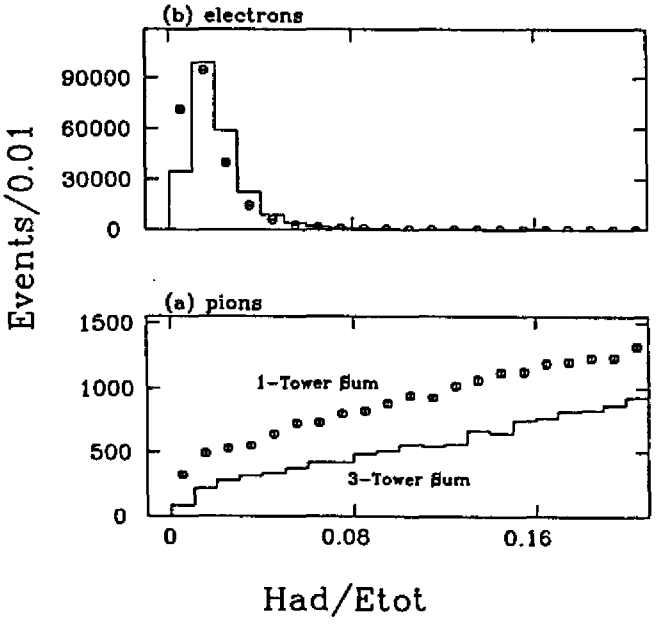

Figure 10

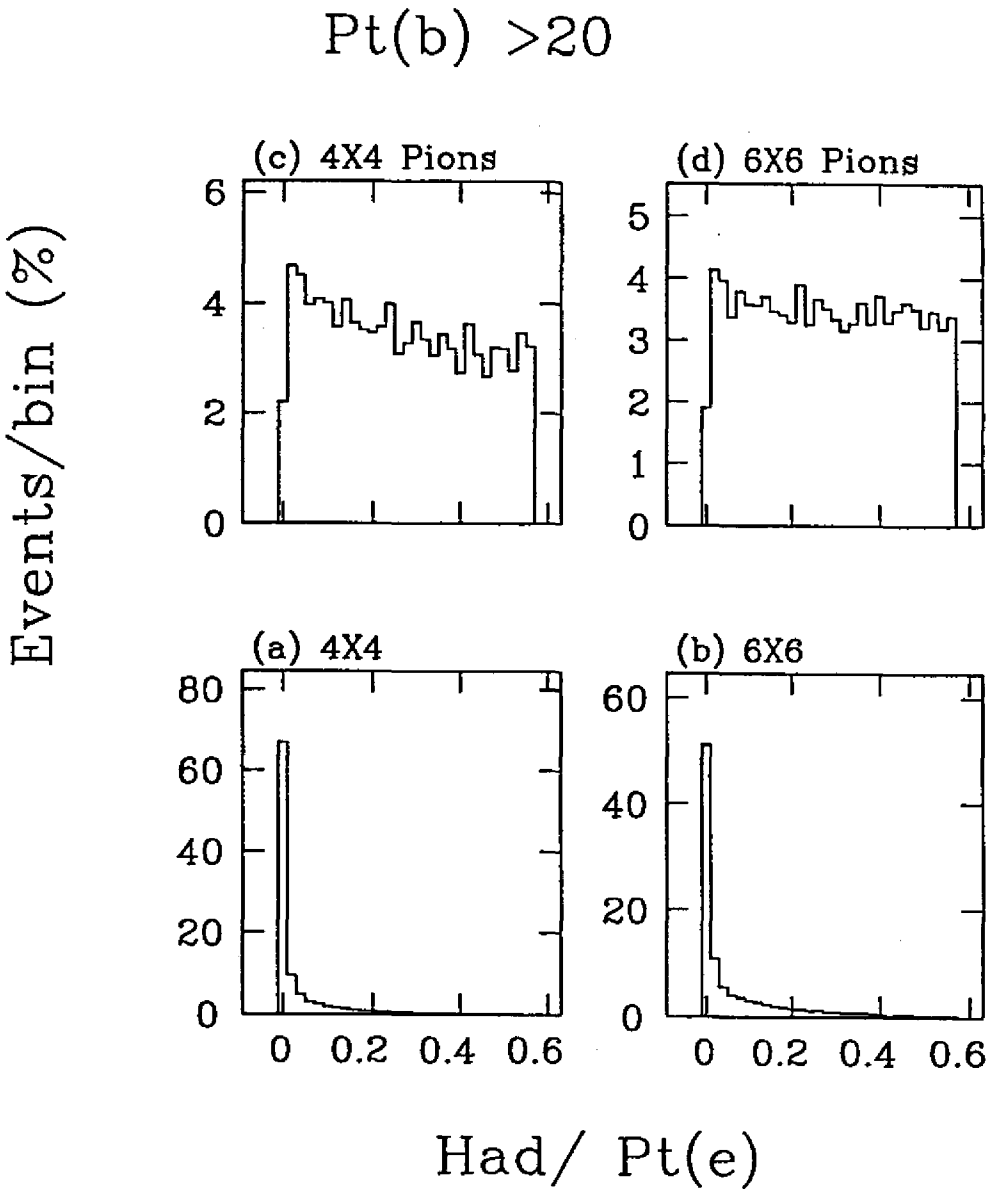
Pt(b) >20
(c) 4X4 Pions
(d) 6X6 Pions
(a) 4X4
(b) 6X6
Events/bin (%)
Had/ Pt(e)
0
0.2
0.4
0.6

Figure 11

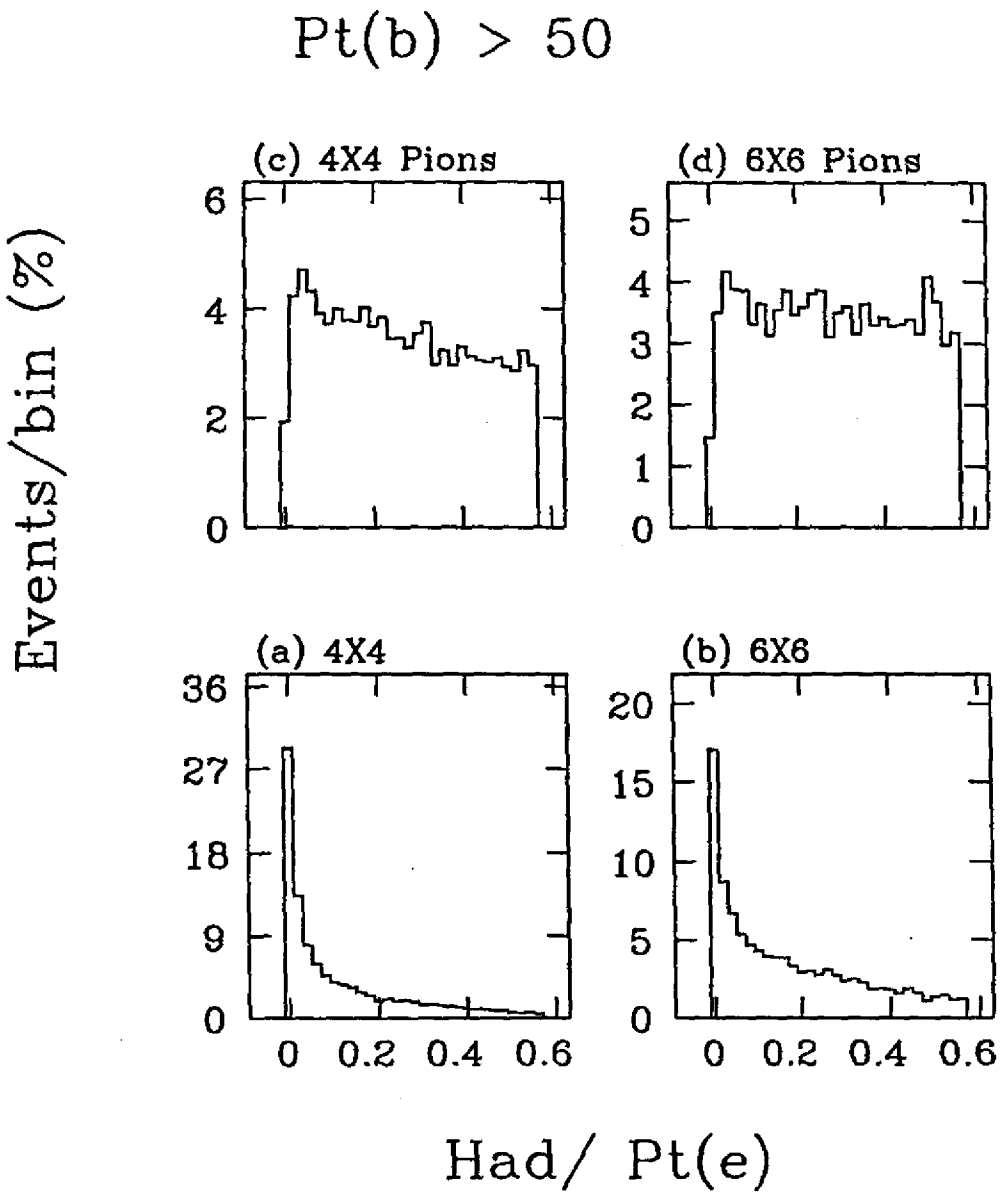
Pt(b) > 50
(c) 4X4 Pions
(d) 6X6 Pions
(a) 4X4
(b) 6X6
Events/bin (%)
Had/ Pt(e)
0
0.2
0.4
0.6

Figure 12

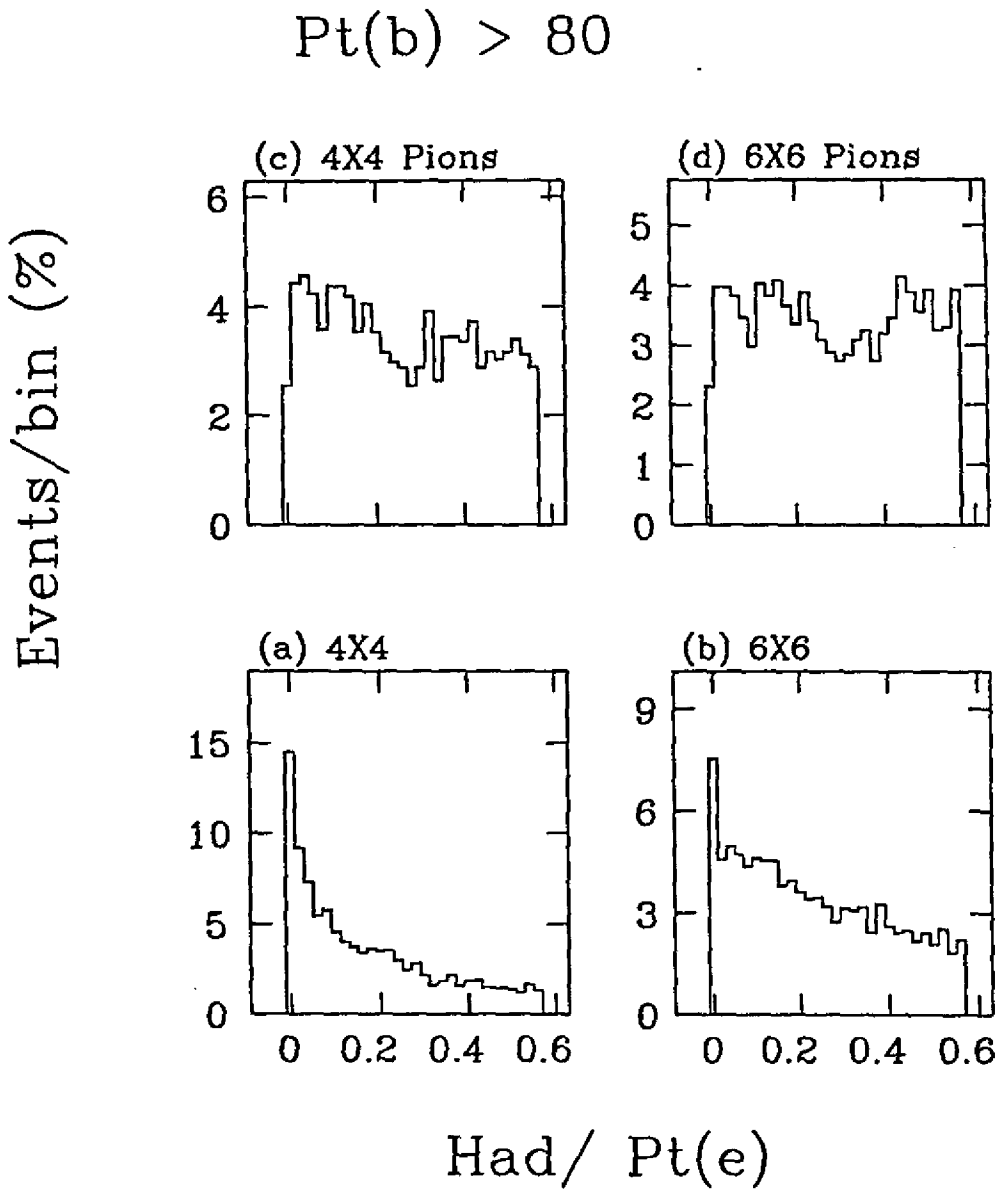
Pt(b) > 80
(c) 4X4 Pions
(d) 6X6 Pions
(a) 4X4
(b) 6X6
Events/bin (%)
Had/ Pt(e)
0
0.2
0.4
0.6

Figure 13

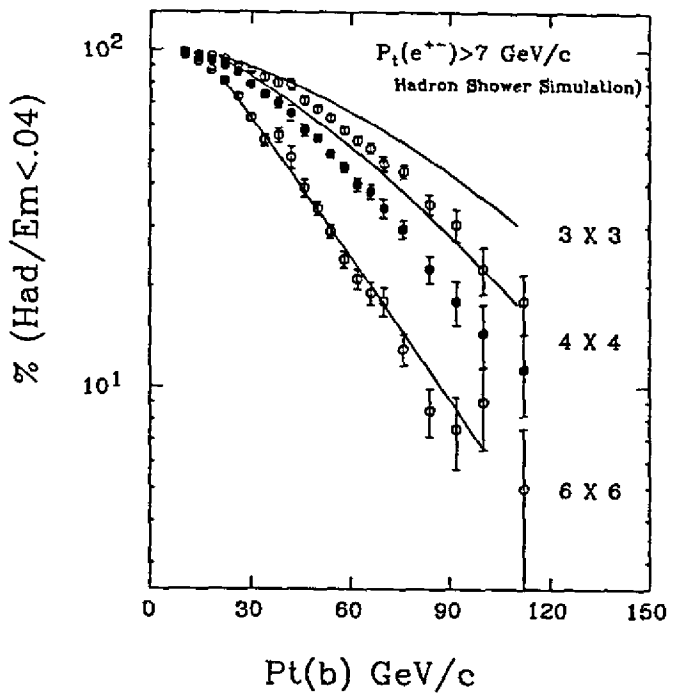

Figure 14

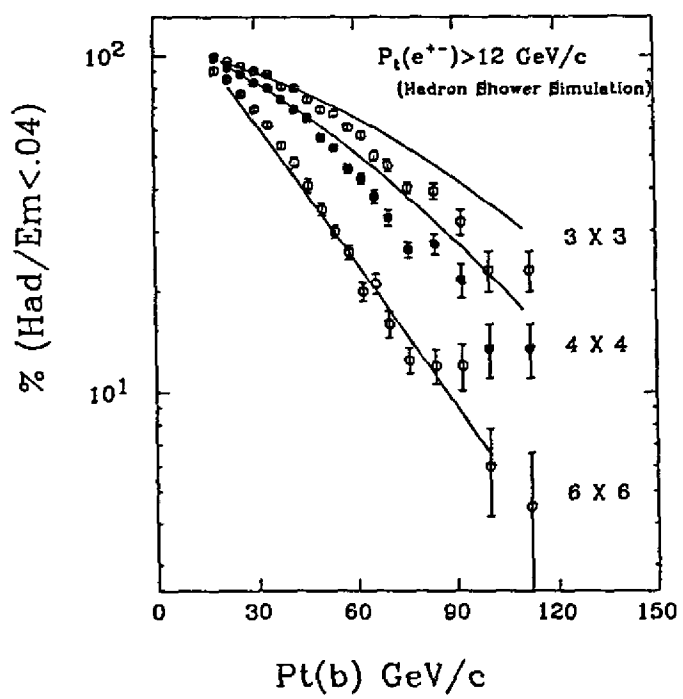

Figure 15

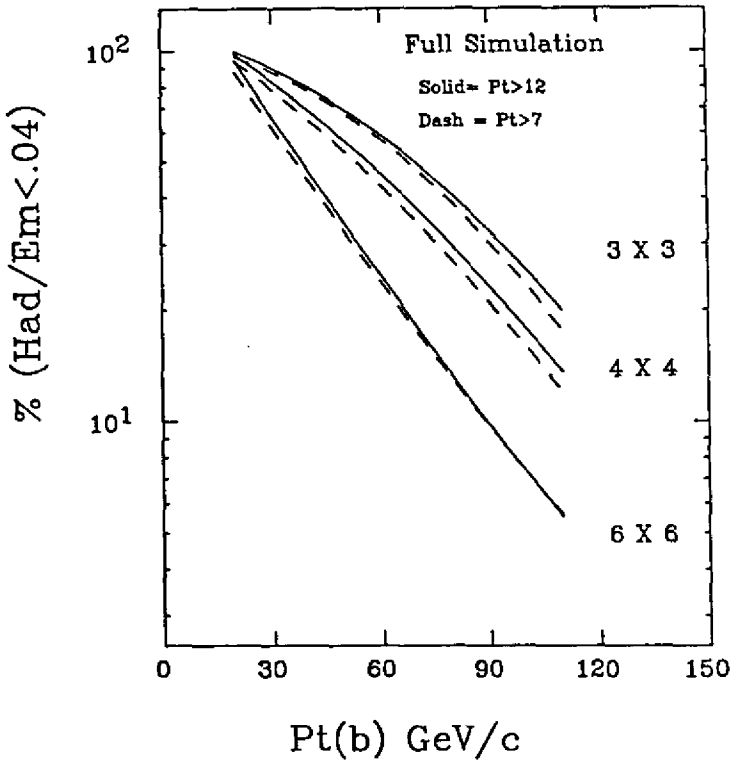

Figure 16

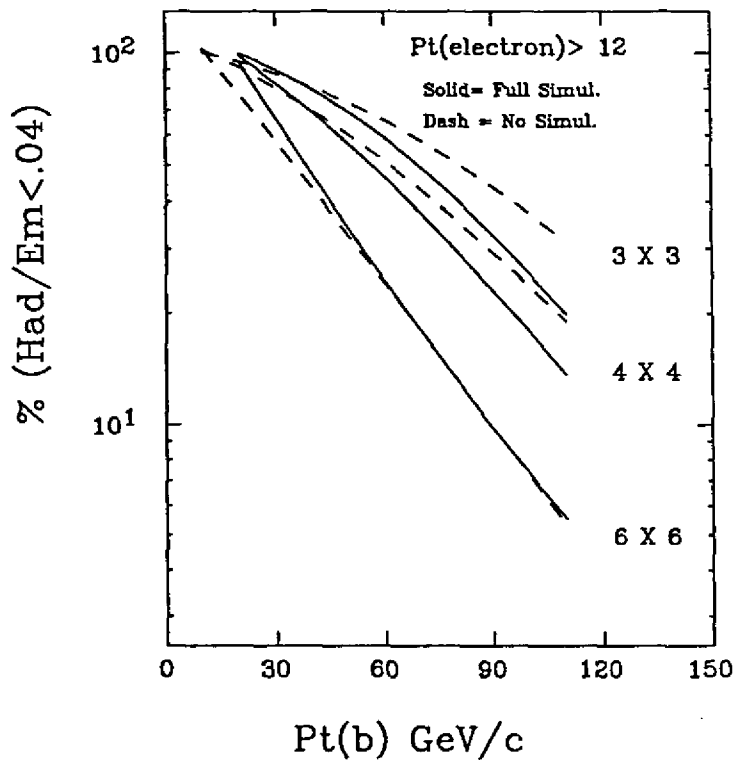

Figure 17

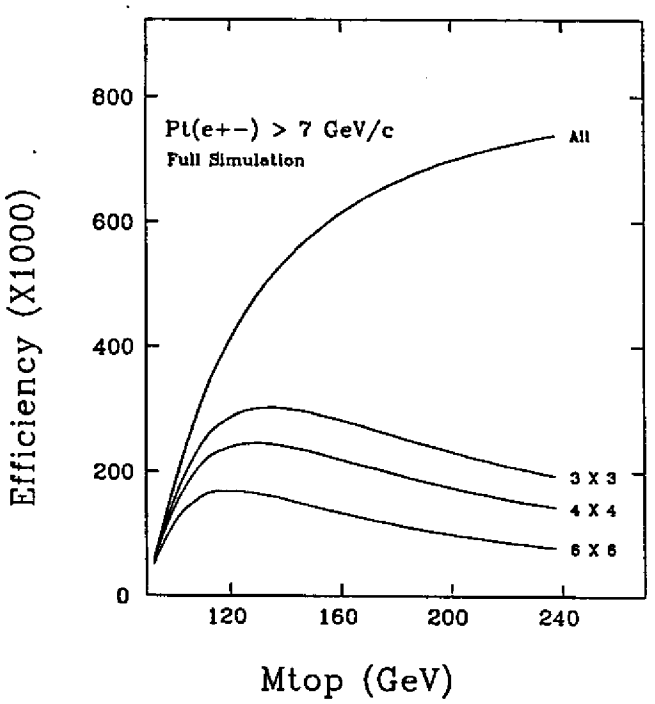

Figure 18

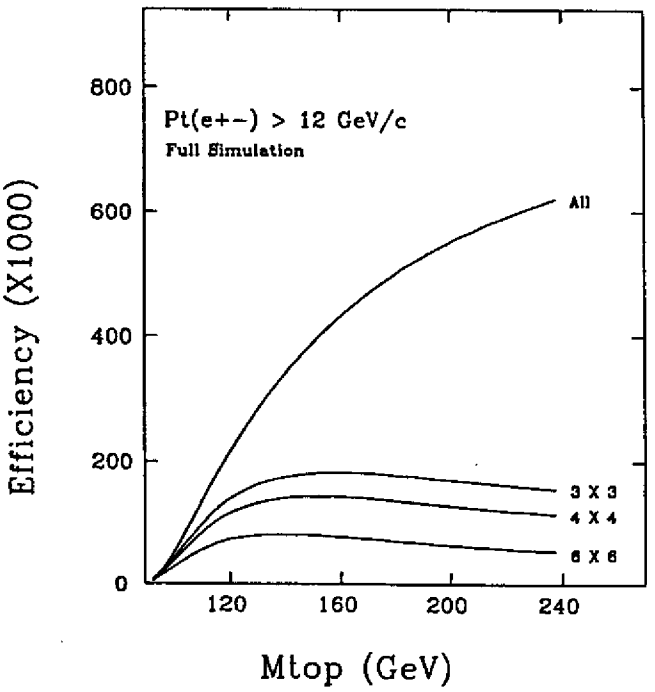

Figure 19